High-performance continuous-wave room temperature 4.0-μm quantum cascade lasers with single-facet optical emission exceeding 2 W

A. Lyakh[a], R. Maulini[a], A. Tsekoun[a], R. Go[a], S. Von der Porten[a], C. Pflügl[b], L. Diehl[b], Federico Capasso[b], and C. Kumar N. Patel[a,c,1]

[a]Pranalytica, Inc., 1101 Colorado Avenue, Santa Monica, CA 90401; [b]School of Engineering and Applied Sciences, Harvard University, Cambridge, MA 02138; and [c]Department of Physics and Astronomy, University of California, Los Angeles, CA 90095

Contributed by C. Kumar N. Patel, September 9, 2010 (sent for review August 26, 2010)

A strain-balanced, AlInAs/InGaAs/InP quantum cascade laser structure, designed for light emission at 4.0 μm using nonresonant extraction design approach, was grown by molecular beam epitaxy. Laser devices were processed in buried heterostructure geometry. An air-cooled laser system incorporating a 10-mm × 11.5-μm laser with antireflection-coated front facet and high-reflection-coated back facet delivered over 2 W of single-ended optical power in a collimated beam. Maximum continuous-wave room temperature wall plug efficiency of 5.0% was demonstrated for a high-reflection-coated 3.65-mm × 8.7-μm laser mounted on an aluminum nitride submount.

high power | midinfrared

Quantum cascade lasers (QCLs) are important infrared light sources with various applications in defense and civilian fields. Low atmospheric absorption in the first atmospheric window spanning from 3.5 to 4.8 μm gives rise to a number of applications based on free light propagation, such as light detection and ranging sensors and beacons. Strong carbon dioxide absorption for wavelengths from 4.2 to 4.4 μm splits the window into two subbands: 3.5–4.2 and 4.4–4.8 μm. Light propagation at wavelengths in either of the two subbands does not experience any significant atmospheric losses. Currently, most of the systems for commercial and defense applications in the wavelength regions rely on expensive and often unreliable optical parametric oscillators (OPOs) or flash lamps as the optical radiation sources. Recent breakthrough developments in continuous-wave (CW) QCL performance at 4.6 μm (1, 2) make them ideal for applications in these systems as light sources in the longer wavelength region of the first atmospheric window. Availability of high-performance QCLs emitting in the shorter wavelength region covering 3.5–4.2 μm, in addition to the high-performance 4.6-μm QCLs, would allow replacing OPOs and flash lamps with compact, reliable, more energy-efficient, and less-expensive QCL systems. However, QCL performance in the shorter wavelength region has lagged significantly behind that of their longer wavelength counterparts. The highest CW room-temperature wall plug efficiency (WPE) and optical power reported, until now, are ∼3% and 500 mW, respectively, for lasers mounted on diamond submounts (3). In the present work, we report significant improvement in 4.0-μm QCL performance and realization of reliable and compact air-cooled 4.0-μm QCL systems capable of delivering over 2 W of optical power in a collimated beam.

One of the reasons for the poorer performance of QCLs at wavelengths shorter than 4.5 μm is carrier leakage from the upper laser level through closely located indirect states. As laser transition energy increases, the upper laser level moves up, approaching the bottom of the indirect band profile corresponding to indirect X or L valleys. Reduced energy spacing between the upper laser level and bottom of indirect valleys increases carrier scattering from the upper laser level to indirect states leading to a reduction in population inversion. Another reason for relatively low, shorter-wavelength QCL performance is thermionic carrier leakage from the upper laser level to continuum states located above barriers due to insufficient bandgap offset of the AlInAs/InGaAs composition (4). Relatively low bandgap offset for AlInAs/InGaAs composition is the reason why QCLs based on AlAsSb/InGaAs composition with significantly higher band offset have received much attention lately, and have shown to provide ∼10% pulsed WPE at room temperature emitting at 3.7 μm (5). Employing the ultimate InAs/AlSb composition, emission wavelengths down to 2.6 μm from QCLs have also been reported (6). However, at wavelengths ∼4.0 μm, AlInAs/InGaAs composition with ∼1.5% strain in AlInAs barriers should provide energy separation between the upper laser level and continuum states equal to or larger than that for the high-performance 4.6-μm QCLs, i.e., ∼250 meV (millielectron volt). In addition, as discussed in ref. 7, it is the indium percentage in InGaAs quantum wells, approximately the same for AlInAs/InGaAs and AlAsSb/InGaAs-based QCL structures at ∼4.0 μm that defines bottom of the indirect band profile and therefore carrier leakage through indirect states. Thus, for wavelengths close to 4.0 μm, no significant advantage is expected in using less mature AlAsSb/InGaAs active regions. In the present work, we used the traditional AlInAs/InGaAs composition for 4.0-μm QCL active region.

Results

In the 4.0-μm active region design, our goal was to reproduce, as closely as possible, design parameters of the high-performance nonresonant extraction 4.6-μm structure reported in ref. 1. A conduction band diagram of two gain stages based on highly strained $In_{0.73}Ga_{0.27}As/Al_{0.71}In_{0.29}As$ composition, very similar to the composition of the 4.0-μm structure reported in ref. 8, is shown in Fig. 1. As with the 4.6-μm structure, energy spacings between levels 5 and 4 (E_{54}), 3 and 1 (E_{31}), and voltage defect, defined as energy spacing between levels 3 and inj ($E_{3\text{-inj}}$) were designed to be approximately 60, 100, and 135 meV, respectively. Energy levels 5, 4, 3, 1, and inj are shown in Fig. 1. Also, doping level in the injector was empirically adjusted so that roll-over current density of the optical power vs. current characteristic was equal to approximately 3 kA/cm^2. This relatively low maximum current density was chosen to reduce active region temperature rise in CW mode operation that is detrimental to CW laser performance. Larger transition energy for the 4.0-μm structure resulted in slightly lower laser transition matrix element (1.37 nm) and larger upper laser lifetime (2.2 ps) compared to the corresponding values for the 4.6-μm structure (1.48 nm and 1.8 ps, respectively). However, the product of matrix element squared and upper laser lifetime, $z^2\tau_4$, the parameter defining differential

Author contributions: C.K.N.P. designed research; A.L., R.M., R.G., S.V.P., C.P., L.D., and F.C. performed research; A.L., R.M., and A.T. analyzed data; and A.L. and A.T. wrote the paper.

The authors declare no conflict of interest.

[1]To whom correspondence should be addressed. E-mail: patel@pranalytica.com.

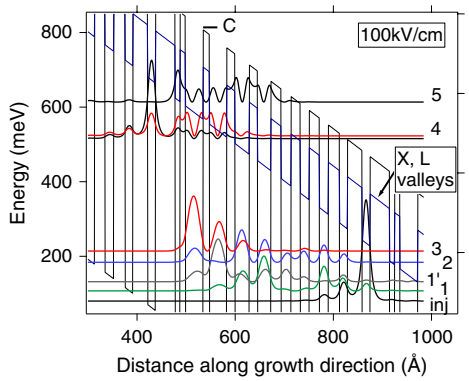

Fig. 1. Band diagram of a quantum cascade laser structure based on $In_{0.73}Ga_{0.27}As/Al_{0.71}In_{0.29}As$ composition and designed using nonresonant extraction principle for light emission at 4.0 μm.

gain, was approximately the same in the both cases. Energy spacing E_{C4} between the upper laser level and continuum states was increased compared to the 4.6-μm lasers from 230 up to 280 meV. Finally, the energy spacing between the upper laser level and bottom of the indirect band profile, calculated at the average upper laser level wavefunction coordinate, was 45 meV. The position of the indirect band profile in this case was determined using model-solid theory results published in ref. 7. The 45-meV energy spacing equals that for the 4.6-μm structure reported in ref. 1. The only difference in positions of indirect valleys between the two structures is that, in the case of the 4.0-μm structure, the bottom of X and L band profiles coincide, whereas for the 4.6-μm structure, the bottom of the L-valley profile is located approximately 30 meV above the bottom of the X-valley profile.

The 40-stage QCL active region, along with the waveguide and contact layer sequence discussed in ref. 9, was grown by molecular beam epitaxy. The wafer was then processed into a buried heterostructure geometry as described in ref. 1 and cleaved into 3.65, 5, and 7 mm long devices. Finally, the laser chips were mounted episide down on aluminum nitride submounts for pulsed and CW characterization. Pulsed testing was performed with 500-ns pulses and 0.5% duty cycle.

Fig. 2, *Inset*, shows the emission spectrum for the lasers at maximum current density in pulsed mode centered at 4.0 μm. Fig. 2 demonstrates that pulsed WPE does not change significantly when laser mirror losses vary between 2.6 and 1.8 cm^{-1} (these losses correspond to losses for 5- and 7-mm-long uncoated lasers, respectively). For CW operation, it is desirable to use devices with lower mirror losses from the optimal 2.6–1.8 cm^{-1} range because they have lower threshold current density in pulsed mode and, as a consequence, lower active region heating close to the laser threshold in CW mode. Fig. 3*A* shows a comparison between pulsed and CW characteristics at 293 K of a 3.65-mm × 8.7-μm high-reflection (HR) coated laser with 1.74 cm^{-1} mirror losses. Threshold current density, slope efficiency, maximum WPE, and maximum optical power in pulsed/CW modes were measured to be 1.207/1.343 kA/cm^2, 3.6/2.1 W/A, 10.5/5.0%, and 2.18/0.75 W, respectively. Five percent is the highest CW WPE from QCLs reported so far at this wavelength at 293 K. Ratio of peak power in pulsed mode to CW maximum power was found to be 2.9, significantly higher than the ratio of 1.6 reported for the 3-mm × 9.5-μm $\lambda = 4.6$-μm laser on aluminum nitride in ref. 1. Fig. 4 *A* and *B* shows that the lower ratio for the 4.0-μm laser can be explained by the lower characteristic temperatures T_0 and T_1 measured for the 4.0-μm laser compared to a 3-mm × 9.5-μm HR-coated 4.6-μm laser processed from the wafer reported in ref. 1. Characteristic temperatures T_0 and T_1 for the 4.0-μm laser were measured to be 135 and 170 K, respectively, vs. 168 and 295 K for the 4.6-μm QCLs. Because E_{54}, E_{31}, $E_{3\text{-inj}}$, and energy spacing between the upper laser level and bottom of indirect states are almost the same for both structures, and E_{C4} is actually larger for the 4.0-μm structure, the 4.6- and 4.0-μm structures are expected to have similar temperature behavior. Parameters defining position of energy levels in Γ-space are well studied and usually provide simulation results consistent with experimental findings. The position of the indirect valleys for strained layers, on the other hand, is much more difficult to predict and not as well studied experimentally. Therefore, a possible explanation for the faster 4.0-μm laser performance degradation with temperature rise is that the actual energy spacing between the upper laser level and bottom of indirect states is lower for the 4.0-μm structure and therefore carrier leakage through indirect states is higher. Another possible explanation is that, because, as described above, the calculated position of the bottom of L-valley profile for the 4.6-μm structure is approximately 30 meV above that for the X valley, carrier scattering to the L valley is suppressed. Higher position of the L valley can lead to lower overall carrier leakage through indirect states for the 4.6-μm design. Employment of even larger strain compositions, with higher position of indirect valleys, should improve 4.0-μm laser thermal characteristic. Suppression of carrier leakage through indirect valleys may help to increase CW wall plug efficiency of these lasers above 10%, similar to performance of the best 4.6-μm structures (1, 2).

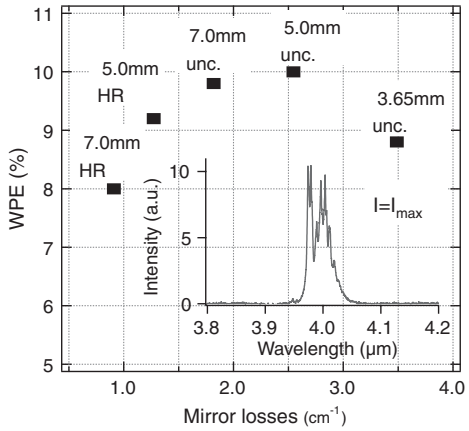

Fig. 2. Dependence of pulsed maximum wall plug efficiency on mirror losses for the uncoated (unc.) and HR-coated 4.0-μm lasers with different cavity length. Inset shows that the spectrum at maximum current is centered at 4.0 μm.

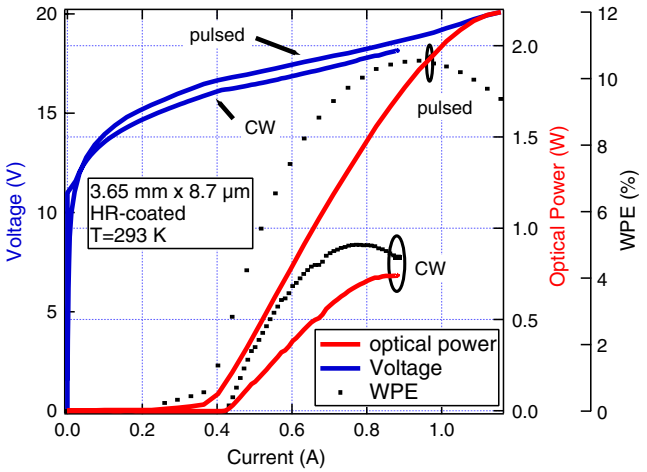

Fig. 3. CW optical power vs. current and voltage vs. current characteristics of an HR-coated 5-mm × 8.7-μm laser measured at 293 K.

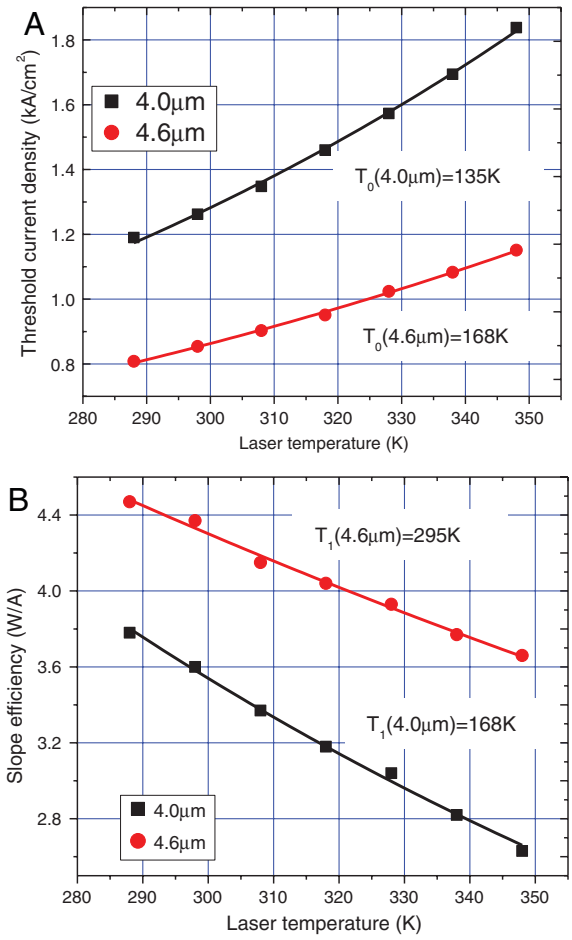

Fig. 4. (*A*) Comparison of threshold current density dependence on laser temperature for the 3.65-mm × 8.7-μm $\lambda = 4.0$-μm laser and the 3.0-mm× 9.5-μm $\lambda = 4.6$-μm laser processed from the structure reported in ref. 1. (*B*) Comparison of slope efficiency on laser temperature for the same lasers.

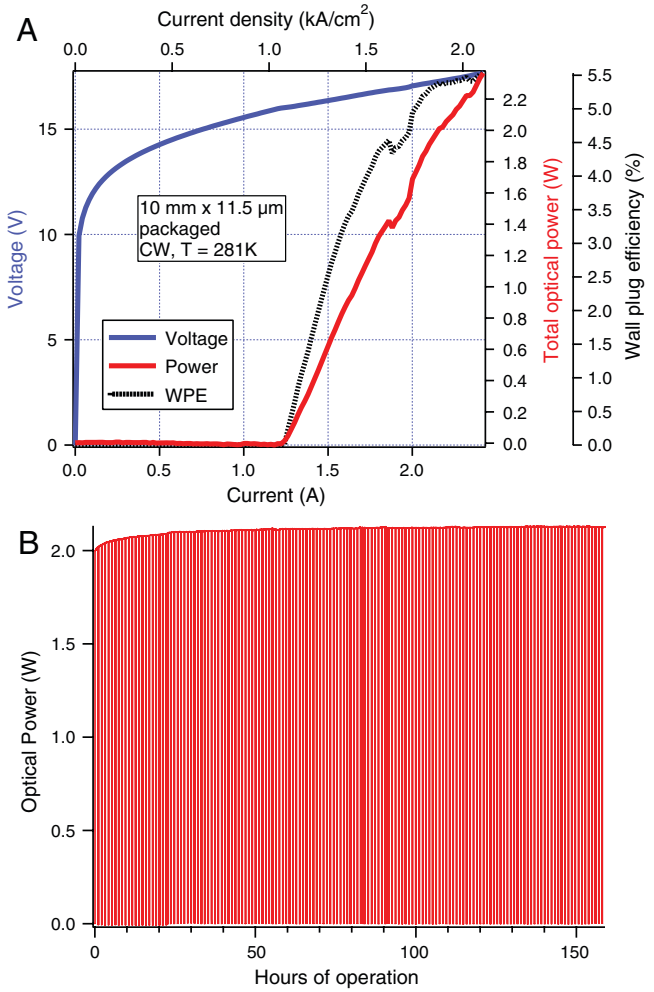

Fig. 5. (*A*) CW and pulsed optical power vs. current and voltage vs. current characteristics measured at 293 K for a hermetically sealed HR/AR-coated 10-mm × 11.5-μm laser. (*B*) Reliability testing of the hermetically sealed laser with periodic power shut downs to induce larger thermal strain.

QCL optical power can be scaled with cavity length employing controlled reflectivity antireflection (AR) coatings, as described in ref. 10. To achieve a multiwatt operation at 4.0 μm, we fabricated an HR-coated 10-mm × 11.5-μm QCL with controlled AR coating adjusted so that the laser had close to optimal mirror losses. This laser was then hermetically packaged and tested on an air-cooled heat sink. The package incorporated a thermoelectric cooler and a collimating lens. Fig. 5*A* shows its CW power vs. current and voltage vs. current characteristics at laser temperature of 281 K and package at room temperature. WPE of 5.5% and optical power of 2.3 W were measured for the laser after correction for the measured 90% collection efficiency of the collimating lens. Fig. 5*B* shows initial reliability testing with periodic hourly laser shut downs to subject the QCL to a large thermal stress (57 min on and 3 min off). Each vertical line in the figure corresponds to laser turn on/off. In several cases, the system had to be shut down before the end of a cycle and then restarted, which is reflected in the reliability data by somewhat heavier lines, when more than one electrical power recycling was done in 1 h. No signs of laser performance degradation were observed after over 150 h of operation. We expect that the long-term reliability of the high-power 4.0-μm QCLs should be similar to what we have already demonstrated for the 4.6-μm high-power QCLs (>3,500 h of performance degradation free operation at CW, room temperature power >2.0 W).

Discussion

In conclusion, we presented experimental data on 4.0-μm QCLs based on the nonresonant extraction approach. WPE of 5.0% was demonstrated at 293 K for an HR-coated 3.65-mm × 8.7-μm laser. Hermetically packaged 10-mm × 11.5-μm HR-coated laser, with the package mounted on an air-cooled heat sink, delivered over 2 W of optical power in a collimated beam. Reliable CW operation was demonstrated for the laser system over 150 h. The 4.0-μm laser systems, owing to their compact size, high WPE, and excellent reliability should be ideal sources in commercial and defense applications requiring ~4.0-μm laser sources.

1. Lyakh A, et al. (2009) 3 watt continuous-wave room temperature single-facet emission from quantum cascade lasers based on non-resonant extraction design approach. *Appl Phys Lett* 95:151112.1–151112.3.
2. Bai Y, Slivken S, Darvish SR, Razeghi M (2008) Room temperature continuous wave operation of quantum cascade lasers with 12.5% wall plug efficiency. *Appl Phys Lett* 93:021103.1–021103.3.
3. Slivken S, Bai Y, Gokden B, Darvish S, Razeghi M (2010) Current status and potential of high power mid-infrared intersubband lasers. *Proc SPIE* 7608:76080B.1–76080B.9.
4. Pflügl C, et al. (2010) Activation energy study of electron transport in high performance short wavelength quantum cascade lasers. *Opt Express* 18:746–753.
5. Commin J, Revin D, Zhang S, Krysa A, Cockburn J (2009) High performance, high temperature ~3.7 μm InGaAs/AlAs(Sb) quantum cascade lasers. *Appl Phys Lett* 95:111113.1–111113.3.
6. Cathabard O, Teissier R, Devenson J, Moreno J, Baranov A (2010) *Appl Phys Lett* 96:141110.1–141110.3.

7. Masselink W, Semtsiv M, Dressler S, Ziegler M, Wienold M (2007) Physics, growth, and performanceof (In,Ga)As–AlP/InP quantum-cascade lasers emitting at $l < 4$ μm. *Phys Status Solidi B* 244:2906–2915.
8. Yu J, et al. (2006) Room-temperature continuous-wave operation of quantum-cascade lasers at $\lambda \sim 4$ μm. *Appl Phys Lett* 88:041111.1–041111.3.
9. Lyakh A, et al. (2008) 1.6 watt, high wallplug efficiency, continuous-wave room temperature quantum cascade laser emitting at 4.6 μm. *Appl Phys Lett* 92:111110.1–111110.3.
10. Maulini R, et al. (2009) High power thermoelectrically cooled and uncooled quantum cascade lasers with optimized reflectivity facet coatings. *Appl Phys Lett* 95:151112.1–151112.3.